DYNAMICAL MODELING OF LARGE SCALE COHERENT STRUCTURES IN THE WAKE OF A WALL MOUNTED FINITE CYLINDER

Zahra Hosseini
Department of Mechanical Engineering
University of Calgary
Calgary, Alberta T2N 1N4, Canada
zhossein@ucalgary.ca

Zixiang Chen
Department of Mechanical Engineering
University of Calgary
Calgary, Alberta T2N 1N4, Canada
zichen@ucalgary.ca

Robert J. Martinuzzi
Department of Mechanical Engineering
University of Calgary
Calgary, Alberta T2N 1N4, Canada
rmartinu@ucalgary.ca

ABSTRACT

The Extended Proper Orthogonal Decomposition (EPOD) was used to estimate the coherent structures in the wake of a wall mounted finite cylinder from the surface fluctuating pressure. To show the surface pressure is actually a good indicator, the method was first applied to the Large Eddy Simulation (LES) results, from which the instantaneous velocity and pressure data were available in the whole domain. Subsequently, the method was applied to planar Particle Image Velocimetry (PIV) measurements for which only the pressure at discrete points at the cylinder side faces were taken. Even though a part of the correlation is lost due to the experimental limitations, the amplitude modulations and base flow variations around the average limit cycle were recovered and great improvements were achieved over the traditional phase averaging approach.

INTRODUCTION

The large scale coherent structures in the wake of a bluff body result in large oscillating pressure loads and vibration on the bluff body and downstream free-standing structures. Aside from engineering applications, due to the formation of vortex structures with different intensities and directions, such flows can be used as benchmarks to evaluate the vortex dynamic models.

The wake of an infinite cylinder is characterized by alternately shed vortices from the sides forming two streets of opposite sign vortices referred to as *Karman vortex street*. In the finite case, due to the interactions with the free shear layer over the obstacle top and the boundary layer at the wall, the structures are highly modified and three dimensional. Consequently, the overall evolution of the structures cannot be easily understood from isolated planar measurements. At the same time, the simultaneous volume measurement of the whole wake is not spatially and temporally well resolved. Bourgeois *et al.* (2011) reconstructed the vortical structures from planar PIV measurements using the traditional phase averaging approach with the phase of the surface pressure as the reference. By this approach, an average over the cycles is forced and the temporal variations of amplitude and base flow around the average limit cycle are categorized as incoherent, even though they have a deterministic character.

In this paper, it is shown that a better representation of the coherent structures can be obtained by using the Extended Proper Orthogonal Decomposition technique (EPOD), Borée (2003). This technique was proposed as a tool to study the correlations between different events in turbulent flows. Herein, the method is used as an estimation technique for the most energetic velocity fluctuating components (i.e., coherent structures). To do so, the conditioning event (sensor or indicator) must be highly correlated with the coherent motions, since the uncorrelated part is lost in the estimation. Sicot *et al.* (2012) showed that the wall pressure can be used as an indicator for the vortical structures developed in the step flow downstream the mean reattachment region. In this work, to check what portion of the energetic motions in the wake are sensed in the pressure data at the wall and the cylinder surface, first the EPOD technique was applied to the instantaneous three-dimensional data obtained from a Large Eddy Simulation (LES) study. The most energetic components were recovered from the pressure, which suggests that there is a high correlation between the surface pressure and the coherent structures. Subsequently, to check the effectiveness of the method within the constraint of experimental limitations, the method was applied to planar velocity data measured simultaneously with the pressure at six locations at the cylinder side faces. The results show that, even though only a discrete set of sensors were available and thus a part of the correlation was lost, the amplitude modulations and base flow variations around the average limit cycle were captured. As a result, a larger portion of coherent energy was recovered compared to the traditional phase averaging approach (where these components of the coherent motions are lost by estimating an average).

EXPERIMENTAL AND COMPUTATIONAL PROCEDURES

Both experimental and computational simulations were performed for a square-cross-section cylinder with height-to-width ratio (Aspect Ratio, AR) $h/d = 4$ mounted on a flat plate. The experiments were also performed for a taller cylinder ($h/d = 8$) for which a higher deviation from the average limit cycle was observed in the wake. In this section the procedure and the set up for experiments and LES study are described.

Experimental Setup

The measurements were conducted in a suction type open-test-section wind tunnel for square-cross-section cylinders with aspect ratio of $h/d = 4$ and 8 ($h = 50.8, 101.6mm$, $d = 12.7mm$) mounted on a sharp-leading-edge flat plate. The boundary layer thickness measured at the location of the cylinder ($x = 200mm$ from the plate leading edge with the cylinder removed) was $\delta/d = 0.72$. The free stream velocity was $U_\infty = 15m/s$, corresponding to a Reynolds number $Re = U_\infty d/\nu = 12,000$, with a free stream turbulence intensity of 0.8%. The measured Strouhal number for both cases was $St = fd/U_\infty = 0.102 \pm 0.003$, with f the vortex shedding frequency. The velocity was measured in two dimensional planes using a LaVision FlowMaster high-frame-rate PIV system. A Photonics Industries 10mJ Nd:YAG laser system was used to form a $1mm$-thick laser sheet. Image pairs with a separation of $50\mu s$ were taken at rates of 500 to 800 (capturing 4 to 7 data points per shedding cycle) by a HighSpeedStar 5 CMOS camera. Interrogation windows of 16×16 with 50% overlap were used to calculate the velocity vectors. For each plane, a minimum of 5000 image pairs were obtained spanning at least 600 shedding cycles. The estimated uncertainty on individual vector measurements is $\Delta u/U_\infty = 0.025$ (Westerweel (2000)).

Simulation Procedure

The simulations were performed for the cylinder with $h/d = 4$ for the same oncoming flow conditions. ANSYS CFX is used for the simulations. Large Eddy Simulation (LES) with the Smagorinsky subgrid-scale model is used. The Smagorinsky Constant is set to 0.1 and von Karman's constant is set to 0.4. Close to the wall, Van Driest wall damping is applied. A finite volume formulation with a Central Difference Advection Scheme and Second Order Backward Euler Transient Scheme was used to discretize the governing equations. The transient simulation is initialized with steady state simulations using the Shear Stress Transport turbulence model. Three levels of grid refinement were carried out. The number of nodes was doubled between levels to ascertain the suitability of the mesh density. A multi-block strategy is employed for meshing. The computational domain consists of 1.4 million hexahedral elements, with about 30 nodes per obstacle diameter. Five hexahedral blocks are extruded from the obstacle free surface to allow enough grid resolution of the obstacle wall shear layers. Inlet and surrounding outlet boundaries are placed at least $2.5h$ away from the location of the obstacle, and an axial distance of $6h$ is allowed for the wake to develop.

COHERENT STRUCTURE MODELING

To isolate the most energetic components of the flow, the Proper Orthogonal Decomposition (POD) was used. The POD is optimal in view that the truncated estimation has the least mean square error compared to other linear decompositions. It is used as an effective tool to obtain a low-dimensional description of high-dimensional data and in the context of turbulent flows is used as an objective method (i.e., does not require *a priori* information) to extract the coherent structures (Lumley (1967)). With the POD, the velocity data are decomposed into purely time-dependent and spatial-dependent parts:

$$\mathbf{u}(\mathbf{X},t) = \sum_{n=1}^{N_{POD}} a^{(n)}(t)\phi^{(n)}(\mathbf{X}) \tag{1}$$

where $\phi^{(n)}$ and $a^{(n)}$ are the n^{th} POD mode and coefficient, respectively. For most applications the number of spatial cells is larger than the time iterations and the POD is found from the snapshot POD approach. In this approach the POD modes are the normalized eigenfunctions of the two-point temporal correlation tensor, and POD coefficients are the projection of the data on the modes (Holmes *et al.* (2012); Tropea *et al.* (2007)). The eigenvalues, λ, represent twice the contribution of each mode to the fluctuating kinetic energy. The modes are ordered in decreasing order of the magnitude of the eigenvalues.

Due to the optimality of the POD space, a relatively small number of modes are sufficient to capture the dominant behaviour of the coherent structures. In this work the first three modes are considered in the analysis as the energy of the rest of the modes are much smaller. For the plane $z/h = 0.25$ (presented in the results section in figure 8), for example, the first three modes capture about 62% and 55% of the total kinetic energy, respectively for $AR = 4$ and 8 cases, and the rest of the energy is distributed among the other 997 modes (number of snapshots $N_t = 1000$).

The Extended POD (EPOD) technique (Borée (2003)) was used to estimate the coherent fluctuations from the surface pressure. To make sure the estimation error is not artificially approaching zero, the dataset used for estimation was different from the data used for assessment (Sicot *et al.* (2012)). For the simulations, the first $N_1 = 2000$ iterations were used to define the extended velocity modes and the next $N_2 = 1000$ iterations were used to check the prediction. For the experiments 4 to 6 trials were available and the prediction was performed on a different trial from those used to find the extended modes.

To obtain the extended modes, first the POD of the pressure data was obtained:

$$P(\mathbf{X},t) = \sum_{n=1}^{N} a_p^{(n)}(t)\phi_p^{(n)}(\mathbf{X}) \tag{2}$$

Then the extended velocity modes, $\psi_\mathbf{u}$, were defined from the temporal correlation of the pressure POD coefficients and the velocity field:

$$\psi_\mathbf{u}^{(n)}(\mathbf{X}) = \frac{\langle a_p^{(n)}(t)\mathbf{u}(\mathbf{X},t)\rangle}{\lambda_p^{(n)}} \tag{3}$$

where $\langle . \rangle$ denotes the time averaging operator. Finally, the velocity was estimated from extended modes and the POD coefficients of the pressure data at a different time interval:

$$\widetilde{\mathbf{u}}(\mathbf{X},t') = \sum_{n=1}^{N} a_p^{(n)}(t')\psi_{\mathbf{u}}^{(n)}(\mathbf{X}) \quad (4)$$

Since the pressure and the velocity field are measured in different domains, there is a phase difference between the velocity POD coefficients and the pressure data. In order to account for this phase shift, a multi-time-delay approach was used (Durgesh & Naughton (2010)). With this approach, to estimate the velocity at each snapshot, pressure from past and future time steps are also used. In other words, at each snapshot the velocity is estimated using the pressure at the same snapshot as well as the pressure signals at past and future times:

$$\widetilde{a}^{(n)} = \langle a^{(n)} \mid p(t_{shift}), t - m\Delta t \leq t_{shift} \leq t + m\Delta t \rangle \quad (5)$$

where $\langle . | . \rangle$ denotes the conditional averaging operator, $\widetilde{a}^{(n)}$ is the estimation of the velocity POD coefficient at time t, Δt is the time step and m is the number of signals considered before and after the estimation time. For the simulations, $m = 15$ corresponding to a time delay $\tau = m\Delta t = 4ms$ was used since for larger time shifts the estimation did not improve significantly. For the experiments, $m = 100 - 200$ corresponding to a time delay $\tau = m\Delta t = 10 - 20ms$ was found to be optimum (not a significant change was observed for higher m values). This larger time delay is expected for the experiments since the pressure was only taken at the cylinder surface. In fact, the time delay is close to the time that it takes for a vortex to travel from the cylinder ($x/d = 0$) to the furthest downstream location ($x/d = 6$) in the plane.

RESULTS

To check the reliability of the conclusions made based on the LES results, the most energetic modes were compared to those obtained from the experiments and overall the trends were similar. Figures 1 and 2 show the POD modes, the Power Spectral Density Function (PSDF) of the corresponding POD coefficients and the contributions to the kinetic energy (normalized by the total kinetic energy obtained from the experiments) at one representative plane $z/h = 0.25$. Although the energy of the small scale fluctuations is predicted higher and decreases less quickly in the simulation results; the energy of the most energetic modes are very close (less than 3% difference). For the purpose of this study, this agreement is sufficient to extend the conclusions from the simulations.

The spectra of the first two modes have a sharp peak at the shedding frequency and compose a harmonic pair representing the periodic nature of the wake. The third mode does not have a peak and is symmetric for u velocity fluctuations. This mode accounts for low frequency variations in the field. This can be seen in figure 3 where the reconstructed velocity fluctuation from this mode is plotted with the original signal. The characteristics of this mode are similar to the *shift mode* defined by Noack *et al.* (2003) as the difference between the steady and the time averaged solution of the Navier Stokes equations. The addition of this mode showed a significant improvement in the transitional behaviour of the estimated wake of an infinite cylinder. In the present case, the first three POD modes were used to reconstruct the coherent fluctuations. The harmonic pair accounts for the periodic motion, and the third mode captures the slow variation of the base flow. The energy level of the higher order modes decreases rapidly and their contribution to the coherent kinetic energy is neglected.

Figure 4 shows the POD modes of the pressure at the wall and the cylinder surface. The characteristics of the modes are similar to those of the velocity field, the first two are a harmonic pair and the third is a symmetric low frequency mode. This correspondence shows the correlation of the surface pressure and the most energetic (coherent) structures in the wake.

The first three spatial modes estimated for the velocity field are shown in figure 5. Note that the modes defined from equation 3 are not normalized (the magnitudes are not unity). To compare them to the POD modes, therefore, they were normalized by their magnitudes and the coefficients were scaled accordingly. The normalized extended modes look very similar to the POD modes (POD modes not shown). The corresponding energy levels, divided by the total kinetic energy obtained from the simulations, are shown in figure 6. Even though the relative fluctuating magnitude of the pressure modes is different from the velocity modes, the relative energy content estimated for the velocity field is intrinsically adjusted by taking the correlation. Even if the order of the pressure modes is different, depending on the locations where the pressure was sampled, the order is recovered in the velocity field.

The instantaneous vortical structures obtained from the reconstructed velocity field is shown in figure 7. For vortex identification, the λ_2 criterion (Jeong & Hussain (1995)) was used. The structures form half loop shapes similar to those obtained from the traditional phase averaging approach (Bourgeois *et al.* (2011)) and those directly from the simulations.

The agreement between the estimation from the wall and cylinder surface pressure and the original simulations shows that the pressure is an effective indicator for the coherent structures (i.e., can be used as the conditioning event for the estimation). Even though there are quantitative discrepancies between the experiments and simulations (Hosseini *et al.* (2013)), this conclusion can be extended to experiments since the main vortical features and overall dynamic trends are captured by the simulations. From the experiments, however, the pressure can only be measured at a discrete set of locations and a part of correlation may be lost. This loss of correlation is more critical for tapered bluff bodies since the interactions between the structures with different frequencies along the span are more significant as they evolve downstream. The ultimate goal of the present work is to enable a structurally and dynamically meaningful comparison between simulations and experimental data and exploit the LES results to arrange the pressure transducers such that this loss is minimized.

For the present dataset, the pressure at 6 locations at the cylinder side faces ($z/h = 0.25, 0.5, 0.75$ at either sides) were taken simultaneously with the planar measurements. Even though the downstream evolution is lost, the estimation is largely improved compared to the traditional phase averaging approach. The estimated energy levels, the phase portrait and the fluctuating signal reconstructed from the first three POD modes (original) and those estimated from the EPOD and traditional phase averaging approach are shown in figure 8 for the cylinders with aspect ratios of 4 and 8 at a horizontal plane $z/h = 0.25$. The energy levels for the traditional phase averaging approach were obtained by performing the POD on the phase averaged field and as expected the shift mode was not captured. For the shorter cylinder, at this plane, the signal is nicely periodic and the traditional phase averaging estimation captures the main dynamical behaviour of the signal. For planes close to the highly reoriented part at the obstacle free-end, where the higher harmonics are not perfect multiples and modulation in the signal is high, the traditional phase averaging results in a poor estimation. The plane shown in figure 8b is an example of a velocity signal with high deviations from the average limit cycle and shows the significant improvement of the EPOD estimation over the traditional phase averaging approach. The amplitude modulations and the base flow drift is captured by the EPOD estimation, and the energy levels estimated for the velocity modes are significantly improved compared to the traditional phase averaging estimation.

CONCLUSION

The correlation of the pressure POD coefficients with the velocity field was used to estimate the dominant behaviour of the coherent fluctuations in the wake of a wall mounted finite cylinder. The amplitude modulation and base flow drift were recovered in the estimation showing that these components of the coherent motion are correlated with the surface pressure. The EPOD technique was shown to be an effective method to find the correlation, even with the limitations of the experimental data. The improvement over the phase averaging approach was shown to be significant when the deviation from the average limit cycle was high. The method can be used to synchronize the planar measurements using the pressure sensors and reconstruct the three-dimensional instantaneous coherent structures. The resultant coherent structures are more representative compared to the traditional phase averaging estimation where only the phase information of the pressure signal is used as the conditioning event and contribution of the deviations from the average cycle is lost.

ACKNOWLEDGEMENTS

The authors would like to thank the Natural Sciences Engineering Research Council of Canada (NSERC) for their financial support of this work.

REFERENCES

Borée, J. 2003 Extended proper orthogonal decomposition: a tool to analyse correlated events in turbulent flows. *Experiments in Fluids* **35**, 188–192.

Bourgeois, J.A., Sattari, P. & Martinuzzi, R.J. 2011 Alternating half-loop shedding in the turbulent wake of a finite-surface-mounted square cylinder with a thin boundary layer. *Physics of Fluids* **23**.

Durgesh, V. & Naughton, J.W. 2010 Multi-time-delay LSE-POD complementary approach applied to unsteady high-Reynolds-number near wake flow. *Experiments in Fluids* **49**, 571–583.

Holmes, P., Lumley, J.L., Berkooz, G. & Rowley, C.W. 2012 *Turbulence, coherent structures, dynamical systems and symmetry*, 2nd edn. University Press, Cambridge: Cambridge Monographs on Mechanics.

Hosseini, Z., Chen, Z. & Martinuzzi, R.J. 2013 Correlation of wall pressure with large-scale structures in the wake of a surface-mounted rectangular cylinder. *CFD Society of Canada* .

Jeong, J. & Hussain, F. 1995 On the identification of a vortex. *Journal of Fluid Mechanics* **285**.

Lumley, J.L. 1967 The structure of inhomogeneous turbulence. *Atmospheric Turbulence and Wave Propagation* pp. 166–178.

Noack, B.R., Afanasiev, K., Morzynski, M., Tadmor, G. & Thiele, F. 2003 A hierarchy of low-dimensional models of the transient and post-transient cylinder wake. *Journal of Fluid Mechanics* **497**, 335–363.

Sicot, C., Perrin, R., Tran, T.T. & Borée, J. 2012 Wall pressure and conditional flow structures downstream of a reattaching flow region. *International Journal of Heat and Fluid Flow* **35**, 119–129.

Tropea, C., Yarin, A.L. & Foss, J.F. 2007 Review of some fundamentals of data processing. *Springer Handbook of Experimental Fluid Mechanics* pp. 1337–1398.

Westerweel, J. 2000 Theoretical analysis of the measurement precision in particle image velocimetry. *Experiments in Fluids* **29**, S3–S12.

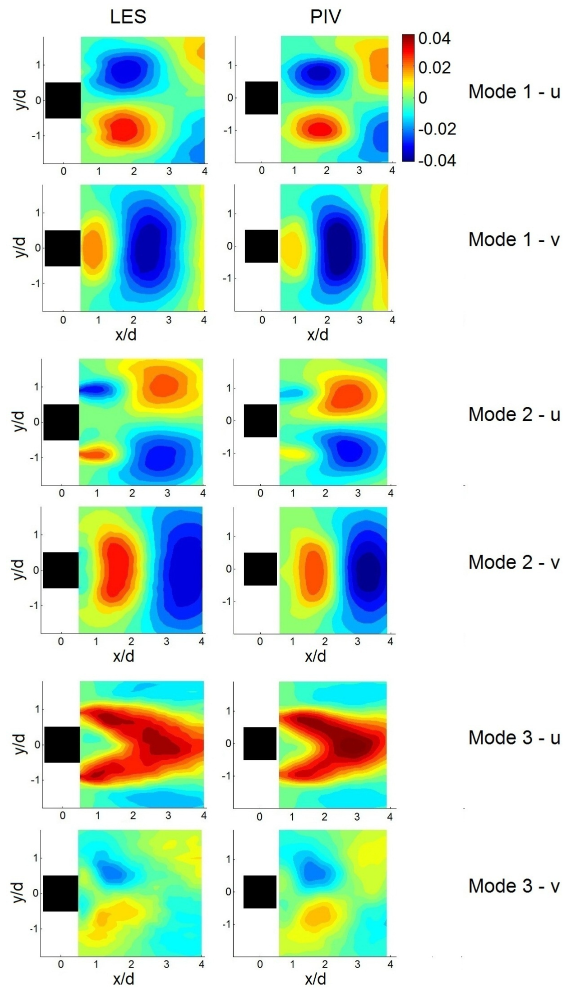

Figure 1: The POD modes for the velocity field at a horizontal plane $z/h = 0.25$ from LES (left) and PIV measurements (right).

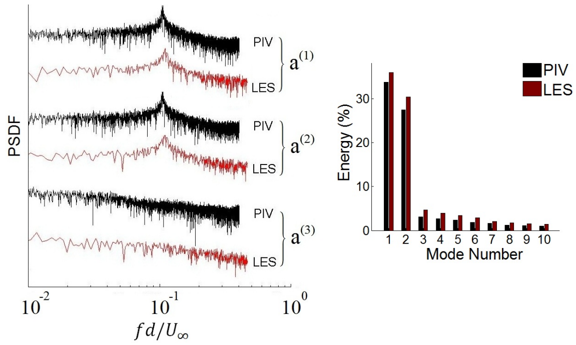

Figure 2: The PSDF of the velocity POD coefficients and the percentage of the energy contribution of the modes at a horizontal plane $z/h = 0.25$ from both LES and PIV measurements. Spectra are offset by multiples of 10 for clarity.

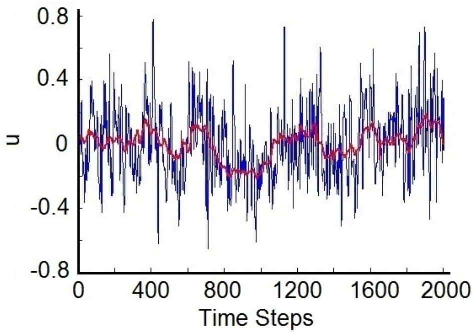

Figure 3: The blue signal shows the total u velocity fluctuation and the solid red line shows the contribution of the third mode capturing the low frequency variations in the signal.

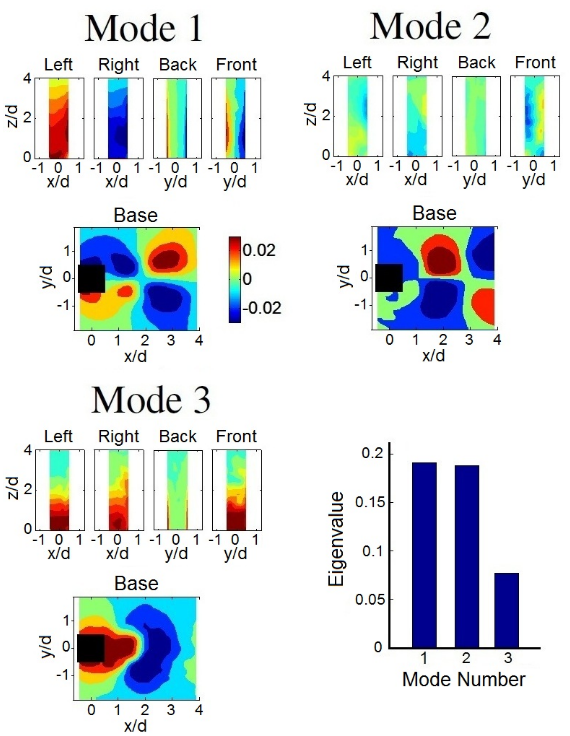

Figure 4: The POD modes for the surface pressure and the POD eigenvalues, λ, normalized by the sum of the λ values.

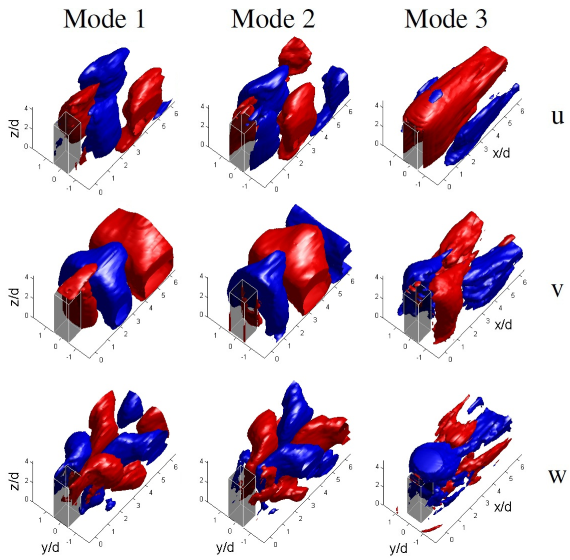

Figure 5: The most energetic modes estimated for the velocity field. For the sake of comparison the modes are normalized.

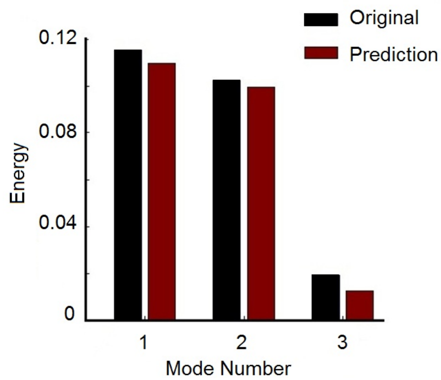

Figure 6: The energies predicted from the surface pressure for the normalized extended modes compared to those obtained directly from POD on the velocity field. The energies are normalized by the total kinetic energy of the velocity field.

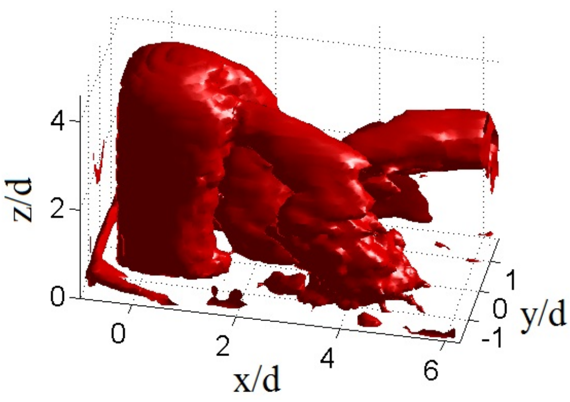

Figure 7: The instantaneous vortical structures obtained from the reconstructed flow from the first three extended modes. For the vortex identification scheme, the λ_2-criterion is used.

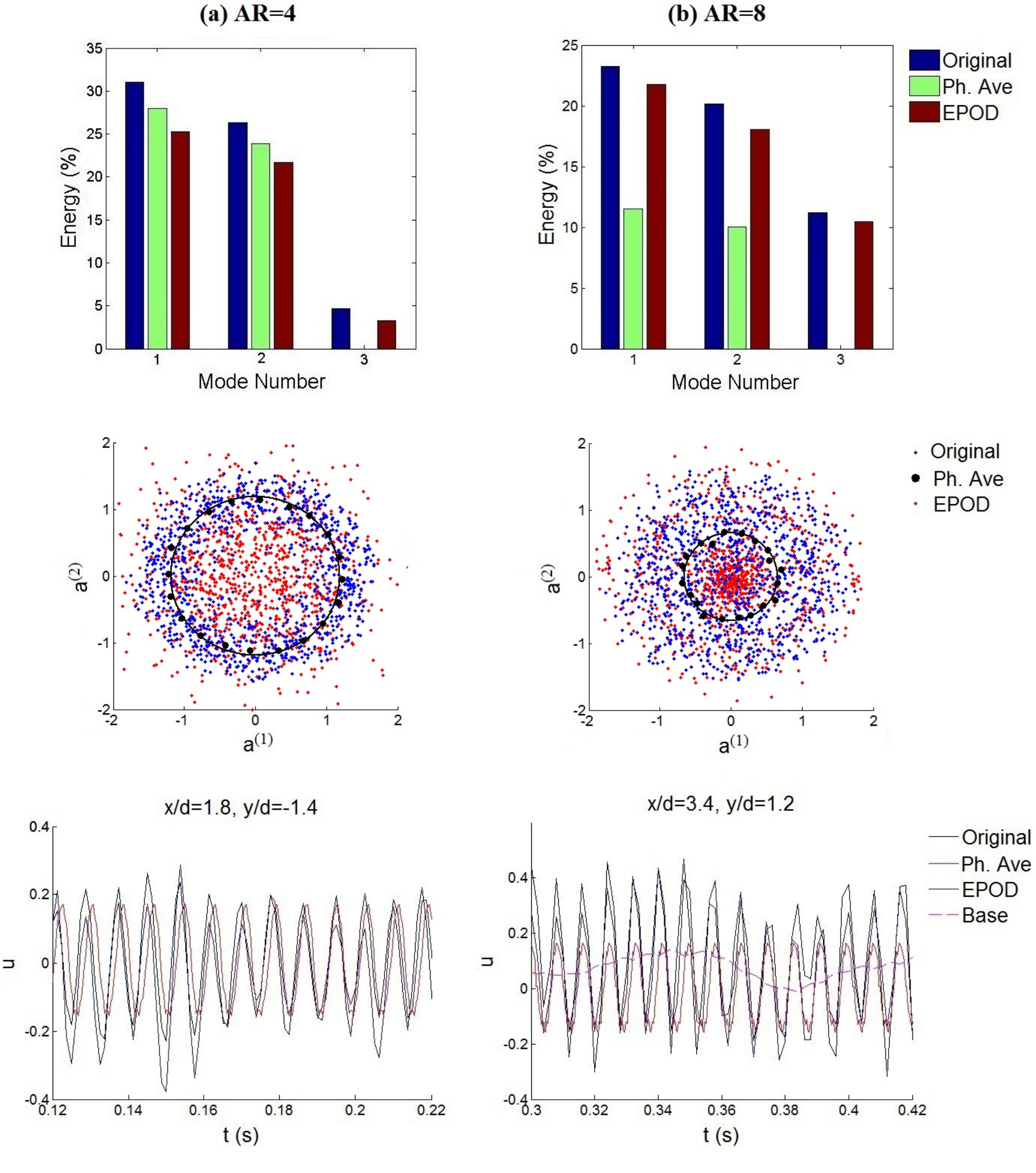

Figure 8: The energy levels for the first harmonic pair and the shift mode, the POD coefficients of the first harmonic pair $(a^{(1)}, a^{(2)})$, and the coherent fluctuations at a point in the wake obtained from the first three POD modes and estimated from phase averaging and EPOD techniques for the cylinders with $AR = 4$ and 8 at $z/h = 0.25$.